

Reykjanes 'V'-shaped ridges originating from a pulsing and dehydrating mantle plume

Garrett Ito

Department of Geology, University of California, Davis, California 95616, USA

Prominent crustal lineations straddle the Reykjanes ridge, south of Iceland (Fig. 1). These giant V-shaped features are thought to record temporal variations in magma production at the Reykjanes ridge axis, associated with along-axis flow of Icelandic plume material¹. It has been proposed that this flow is channelled preferentially along the ridge axis²⁻⁴, and that temporal variability is induced by fluctuations of the Iceland plume itself^{4,7} or, alternatively, by relocations of the ridge axis on Iceland⁸. Here I present a geodynamic model that predicts the formation of crustal V-shaped ridges from a pulsing and radially flowing mantle plume. In this model, plume pulses produce mantle temperature perturbations that expand away from the plume in all directions beneath the zone of partial melting. The melting zone has a high viscosity owing to mantle dehydration at the onset of partial melting⁹. This high-viscosity region allows for reasonable variations in crustal thickness, produces crustal Vs that extend hundreds of kilometres along the axis, and prevents the plume material from being preferentially channelled along the ridge axis. The angle of the crustal V-shaped features relative to the ridge axis reflects the rate of lateral plume flow, which remains several times greater than the ridge half-spreading rate over the length of a crustal V. Consequently, this radially expanding plume produces lineations in crustal thickness and free-air gravity anomalies that appear to be nearly straight.

This model builds on previous three-dimensional numerical simulations of a ridge-centred plume^{10,11}. Mantle convection is simulated by solving the equations describing conservation of mass, momentum and energy in a fluid of zero Reynolds number and moderately temperature-dependent viscosity¹². An essential feature of this model is an increase in viscosity by a factor of 100 near the base of the primary melt production zone. Such an increase in viscosity is likely to occur as water is extracted from the mantle at the very early stages of decompression partial melting⁹.

The mantle flow and temperature distribution of a steady-state, ridge-centred plume is shown in Fig. 2a. Low-viscosity and thermally buoyant plume material rises beneath the ridge axis, spreads laterally beneath the high-viscosity melting zone, and attains a steady-state, along-axis width^{10,11,13,14}. In the overlying melting zone, high viscosities minimize along-axis and vertical flow, and upwelling occurs primarily to accommodate the spreading of the two plates. This slow, passive upwelling allows a plume of relatively high excess temperature and narrow radius^{15,16} to produce crustal thicknesses¹¹ that are consistent with seismic observations on Iceland (for example, see refs 17 and 18).

I now vary the volume flux of upwelling plume material as a periodic function in time. This is done by varying the imposed radius of the plume stem about the steady-state value of 100 km. The period of variation of 8 Myr is in the range of 5–10 Myr estimated for the age contrasts between adjacent V-shaped ridges in the North Atlantic Ocean^{14,19}. A possible cause for such flux perturbations is the surfacing of solitary waves in the Iceland mantle plume. Solitary waves have been shown to be stable features that initiate from perturbations in ascending plumes of buoyant viscous fluid^{20,21}. The maximum temperature anomaly of the plume stem remains constant.

The flux variations generate pulses in the plume that rise up the stem and expand outward beneath the boundary at which viscosity increases due to dehydration. Figure 2 shows temperature and flow at three time steps of a calculation in which the plume flux varies between $(6.5 \pm 4.9) \times 10^6 \text{ km}^3 \text{ Myr}^{-1}$. At a time of 2 Myr after the initiation of pulsing, the plume has reached its maximum radius. Because the stem is wider than the steady-state model, a greater volume of hot material flows more rapidly up the plume stem. At positions near the outer portions of the stem, material is hotter than in the steady-state model because of the greater plume width. Temperatures at the centre of the stem are unchanged. The leading portion of the pulse has already struck the dehydration boundary and has begun to expand away from the plume stem as an annulus of hotter-than-normal material.

At 4 Myr the basal radius of the plume stem has returned to the steady-state value and the pulse is now expanding away from the plume stem beneath the dehydration viscosity boundary (Fig. 2c). Compared to the steady-state condition, the 1,450 and 1,500 °C isotherms extend a greater radial distance from the centre of the plume, indicating hotter material in these regions. Temperature perturbations are greatest (the maximum is +56 °C) at radial distances of ~75–375 km. A cross-section at a depth of 135 km shows that temperature perturbations diminish with distance away from the ridge axis. This is a result of conductive cooling beneath a plate of increasing age.

Finally, at 7 Myr the plume stem is in a contracted form (Fig. 2d). Material surrounding this thinner plume stem is cooler than in the steady-state model and an annulus of cooler-than-normal material is expanding away from the stem beneath the dehydration boundary. The original, high-flux pulse is now 300–500 km away from the plume stem, though the magnitude of temperature perturbations has

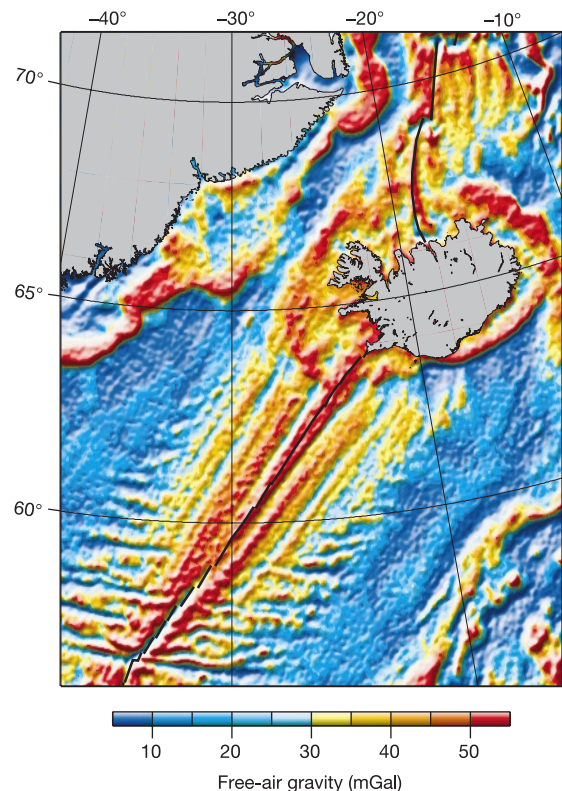


Figure 1 Satellite-derived free-air gravity anomalies in region surrounding Iceland²⁷. Reykjanes ridge is the linear high (bold line) that bisects V-shaped features pointing southward from Iceland. Similar though less regular lineations are also evident near the Kolbeinsey ridge to the north.

diminished (the maximum is +35 °C). At later times, this pulse will continue to radiate away from the plume stem until its effects are minimal beyond a distance of ~600 km. The cooler-than-normal material will follow the leading pulse and then a new high-flux pulse will rise to start a new cycle.

The above dynamics result in alternating high and low tempera-

ture perturbations that propagate along the ridge axis beneath the partial melting zone. This model thus presents a mechanism for generating variations in mantle temperature, as described in ref. 4, and magma production anomalies that propagate along-axis, as first conceptualized in ref. 1. The pattern of crustal thickness predicted by assuming all melts produced in the mantle migrate

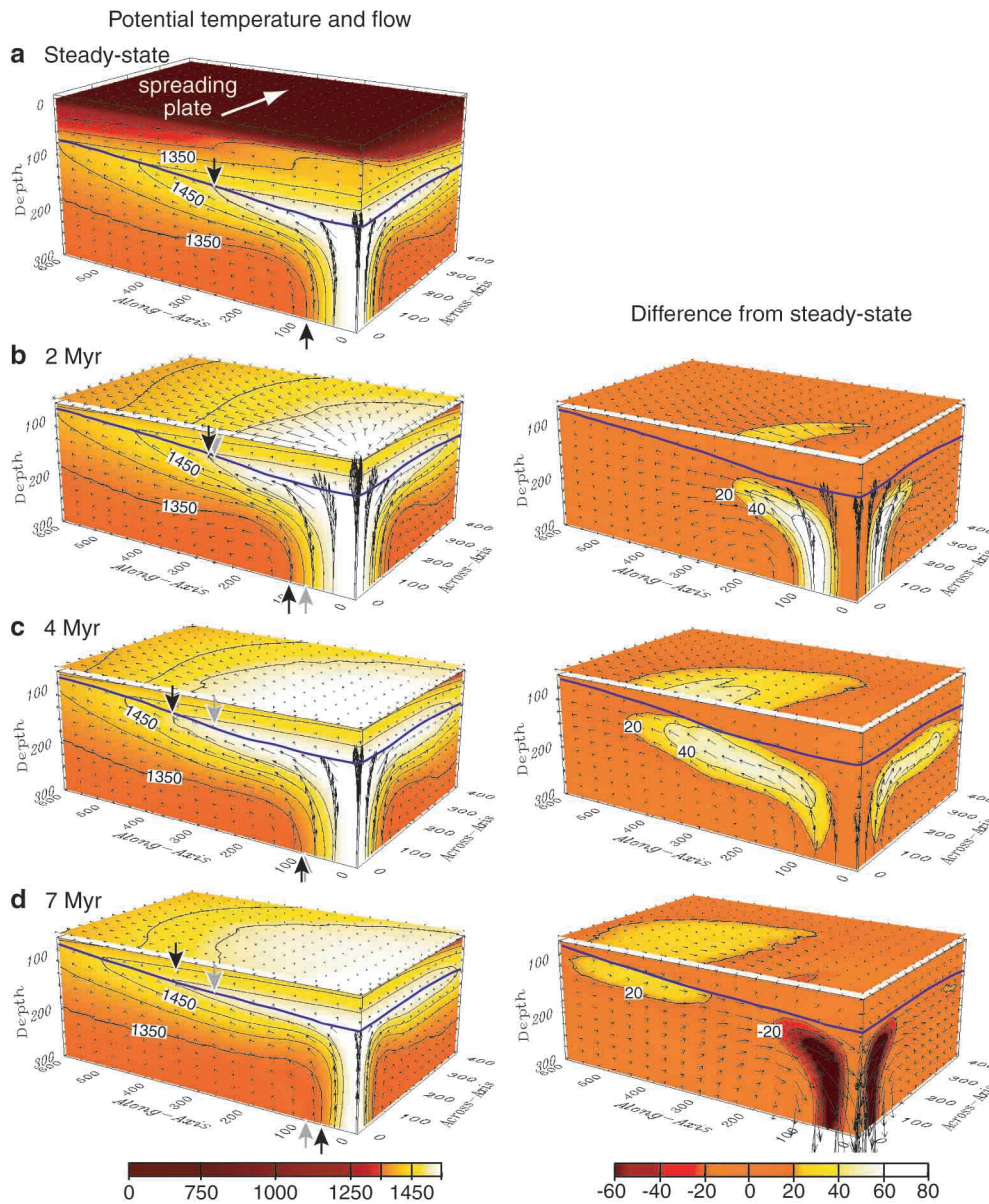


Figure 2 Potential temperatures and flow fields (left) and differences from the steady-state model (right). Potential temperatures (contour interval 100 °C) and flow (arrow size proportional to flow rate) are shown on the left, and differences in temperature (contour interval 20 °C) and flow from the steady-state plume model (arrows point down if ascent is slower than in steady-state model) are shown on the right. The left vertical panels are along the ridge axis; the right vertical panels are perpendicular to the ridge axis. The box sides are reflecting boundaries and the tops and bottoms (except in the plume) have uniform potential temperatures of 0 and 1,350 °C, respectively. Plate spreading is simulated by imposing a constant horizontal velocity (the half-spreading rate is 9.5 km Myr⁻¹; ref. 28) at the surface of the box, and the plume is generated by imposing a cylindrical temperature anomaly (decreases as a gaussian function from a maximum of 200 °C to 5 °C at specified plume radius) in the lower portion of the box. The ambient (reference) viscosity at a depth of 250 km is 5 × 10¹⁹ Pa s; the minimum viscosity in the

plume is 5.8 × 10¹⁸ Pa s; and the cut-off maximum viscosity is 2.5 × 10²² Pa s. Dehydration viscosity increase (boundary marked by bold blue curve) is incorporated by a pre-exponential multiplying factor¹¹ that increases from 1 to 100 over mantle depletions of 0 to 5%. Melting calculations are based on ref. 29. The boxes have across-axis, along-axis and vertical dimensions 1,152 × 1,152 × 500 km; number of grids are 162 × 128 × 100. **a**, Steady-state plume beneath ridge axis. Upper bold arrow marks along-axis extent of 1,500 °C isotherm; lower bold arrow marks boundary of plume stem. **b**, 2 Myr after the initiation of plume flux perturbation. Horizontal cross-section is at a depth of 145 km. Bold arrows show new extent of 1,500 °C isotherm and plume stem boundary; grey arrows show corresponding positions in the steady-state model (separation between bold and grey arrows indicate changes in temperature). **c**, Time is 4 Myr and horizontal cross-section is at a depth of 135 km. **d**, Time is 7 Myr and horizontal cross-section is at a depth of 130 km.

perpendicularly towards the ridge axis to form crust is illustrated in Fig. 3a. Superimposed on a long-wavelength thinning of the crust away from the plume are shorter-wavelength lineations that angle toward the ridge axis in the form of nested Vs. The maximum variation in crustal thickness occurs at an along-axis distance from the plume centre of about 200 km and decreases to nearly zero at a distance of approximately 600 km. Both the distance of maximum variation and the length of the V-shaped ridges remain nearly constant among models in which plume flux is perturbed by different amounts (the flux range examined here is 46% to 171% of the medians).

The quantity that is most sensitive to changes in flux perturbation is the magnitude of crustal thickness variation. The crustal thickness pattern in Fig. 3a is the predicted by a model in which the plume flux was varied by $(6.1 \pm 2.6) \times 10^6 \text{ km}^3 \text{ Myr}^{-1}$, or a total variation of 83% of the indicated median value. The maximum crustal thickness variation in this calculation is 4.9 km, a value slightly greater than, but comparable to, the range of 2–4 km inferred in ref. 4. A predicted linear increase in maximum crustal thickness variation

with normalized flux variation (Fig. 4) suggests that the crustal thickness variation estimated for the North Atlantic requires substantial flux perturbations of the Iceland plume (34–68% of the median flux). The model also predicts an approximately 3-km variation in crustal thickness over Iceland, and indeed there is stratigraphic evidence that crustal productivity on Iceland has varied at periods comparable to those modelled here^{22,23}.

Figure 3b shows the predicted free-air gravity anomaly that results if the crust is compensated by Airy isostasy (see legend for details). The sensitivity of free-air gravity anomalies to the shorter-wavelength variations in crustal thickness yields prominent V-shapes. The predicted gravity lineations have maximum amplitudes of 35 mGal and lengths of about 600 km, both of which are comparable to observations in the North Atlantic⁴.

It is interesting that the crustal and gravity lineations appear nearly straight. Assuming that the crustal Vs in the North Atlantic formed on the ridge axis, the tangent of the angle between a lineation and the ridge axis is the ratio of the ridge half-spreading rate and the along-axis flow rate of a melt perturbation¹. Previous workers have argued that the apparent straightness of the gravity features indicates a constant along-axis flow rate, which would not occur by radial expansion of plume material^{1,4}. Indeed, as suggested by Vogt¹, the models presented here predict the rate of along-axis flow to decrease in proportion to the inverse of radial distance from the plume centre. Consequently, the predicted V-shaped ridges curve. But they do not curve much. The calculation that produced Fig. 3 has an along-axis plume flow rate that is a maximum of 168 km Myr^{-1} at an along-axis distance of 100 km from the plume centre and decreases to 28 km Myr^{-1} at a distance of 600 km. These flow rates predict the angle between a crustal V and the ridge axis to increase from 3° to 19° . This small change in angle is evident in curves computed from the maximum along-axis flow rates, which closely follow the peaks of the crustal Vs (Fig. 3). In the North Atlantic, the gravity lineations are even longer (Fig. 1), estimated flow rates ($\sim 200 \text{ km Myr}^{-1}$; ref. 1) are greater, and thus bends in crustal Vs are likely to be even smaller than predicted by the above model. Indeed, small bends have been identified in sea-floor basement topography¹.

Finally, I discuss the importance of the rheological boundary caused by mantle dehydration. First, the rheological boundary is a requirement for the formation of elongate V-shaped crustal ridges. Numerical calculations that omit dehydration predict dramatic

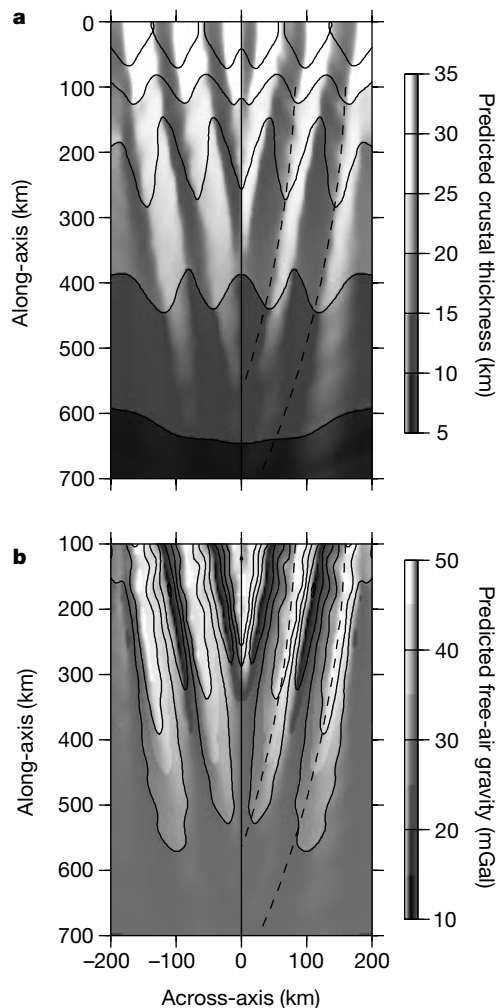


Figure 3 Maps of (a) predicted crustal thickness (contour interval 5 km) and (b) free-air gravity anomaly (contour interval 10 mGal) predicted from crustal structure. Illumination is from the right. Topography of crust–water and crust–mantle interfaces computed by assuming Airy isostatic compensation of crust. The gravitational attraction of the two interfaces was computed²⁰ and then summed. I assumed an upper crustal density of $2,700 \text{ kg m}^{-3}$, a lower crustal density of $3,000 \text{ kg m}^{-3}$ (ref. 4), and a flat interface separating the two. Assumed water and mantle densities are $1,000$ and $3,300 \text{ kg m}^{-3}$, respectively. Solid lines mark ridge axis; dashed curves show trajectory of V-shaped ridges predicted from maximum along-axis flow rates.

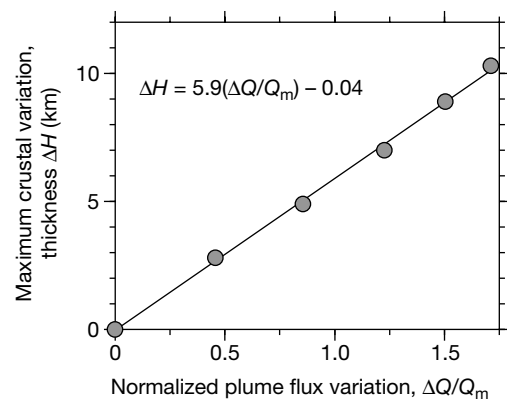


Figure 4 Maximum crustal thickness variations (dots) predicted by models of different variation in plume flux. Flux perturbation is given as difference between maximum and minimum flux ΔQ , normalized by median value Q_m . In order of increasing crustal thickness variation, median fluxes and variations (given as $\pm \Delta Q/2$) are $(5.5 \pm 0) \times 10^6 \text{ km}^3 \text{ Myr}^{-1}$; $(5.7 \pm 1.3) \times 10^6 \text{ km}^3 \text{ Myr}^{-1}$; $(6.1 \pm 2.6) \times 10^6 \text{ km}^3 \text{ Myr}^{-1}$; $(6.2 \pm 3.8) \times 10^6 \text{ km}^3 \text{ Myr}^{-1}$; $(6.5 \pm 4.9) \times 10^6 \text{ km}^3 \text{ Myr}^{-1}$; $(6.8 \pm 5.8) \times 10^6 \text{ km}^3 \text{ Myr}^{-1}$. Line is the indicated best-fitting function.

variations in upwelling rate above the plume stem, which lead to unrealistically large crustal thickness variations (>200 km). Most of the variation is confined to the plume stem and prominent V-shaped ridges fail to form. Secondly, the depth of the dehydration boundary does not increase significantly away from the ridge axis (Fig. 2a). This prevents the formation of a rheological groove from the off-axis thickening of a thermally controlled lithosphere, which could otherwise channel plume material along the ridge axis for very-low-viscosity plumes²⁴. Flow away from the plume stem is therefore nearly radial. This model thus demonstrates how a radially expanding and pulsing plume can generate Reykjanes V-shaped ridges as well as similar sea-floor age-transgressive ridges south of the Azores hotspot^{25,26}. The possibility of a high-viscosity dehydration layer at other plume-ridge systems has broad implications for the fundamental dynamics of plume-ridge interaction as well as asthenosphere-lithosphere interaction in general. □

Received 13 October 2000; accepted 30 March 2001.

- Vogt, P. R. Asthenosphere motion recorded by the ocean floor south of Iceland. *Earth Planet. Sci. Lett.* **13**, 153–160 (1971).
- Schilling, J.-G. Upper mantle heterogeneities and dynamics. *Nature* **314**, 62–67 (1985).
- Vogt, P. R. Plumes, subaxial pipe flow, and topography along the mid-ocean ridge. *Earth Planet. Sci. Lett.* **29**, 309–325 (1976).
- White, R. S., Brown, J. W. & Smallwood, J. R. The temperature of the Iceland plume and origin of outward propagating V-shaped ridges. *J. Geol. Soc. Lond.* **152**, 1039–1045 (1995).
- Hanan, B. B. & Schilling, J.-G. The dynamic evolution of the Iceland mantle plume: the lead isotope perspective. *Earth Planet. Sci. Lett.* **151**, 43–60 (1997).
- Schilling, J.-G. & Noe-Nygaard, A. Faeroe-Iceland plume: Rare-earth evidence. *Earth Planet. Sci. Lett.* **24**, 1–14 (1974).
- Schilling, J. G., Meyer, P. S. & Kingsley, R. H. Evolution of the Iceland hotspot. *Nature* **296**, 313–320 (1982).
- Hardarson, B. S., Fitton, J. G., Ellam, R. M. & Pringle, M. S. Rift relocation—a geochemical and geochronological investigation of a palco-rift in northwest Iceland. *Earth Planet. Sci. Lett.* **153**, 181–196 (1997).
- Hirth, G. & Kohlstedt, D. L. Water in the oceanic upper mantle: Implications for rheology, melt extraction, and the evolution of the lithosphere. *Earth Planet. Sci. Lett.* **144**, 93–108 (1996).
- Ito, G., Lin, J. & Gable, C. W. Dynamics of mantle flow and melting at a ridge-centered hotspot: Iceland and the Mid-Atlantic Ridge. *Earth Planet. Sci. Lett.* **144**, 53–74 (1996).
- Ito, G., Shen, Y., Hirth, G. & Wolfe, C. Mantle flow, melting, and dehydration of the Iceland mantle plume. *Earth Planet. Sci. Lett.* **165**, 81–96 (1999).
- Gable, C. W. *Numerical Models of Plate Tectonics and Mantle Convection in Three Dimensions*. Thesis, Harvard Univ. (1989).
- Feigner, M. A. & Richards, M. A. The fluid dynamics of plume-ridge and plume-plate interactions: an experimental investigation. *Earth Planet. Sci. Lett.* **129**, 171–182 (1995).
- Ribe, N., Christensen, U. R. & Theissing, J. The dynamics of plume-ridge interaction. 1. Ridge-centered plumes. *Earth Planet. Sci. Lett.* **134**, 155–168 (1995).
- Allen, R. M. *et al.* The thin hot plume beneath Iceland. *Geophys. J. Int.* **137**, 51–63 (1999).
- Wolfe, C., Bjarnason, I. T., VanDecar, J. C. & Solomon, S. C. Seismic structure of the Iceland mantle plume. *Nature* **385**, 245–247 (1997).
- Menke, W., Brandsdóttir, B., Einarsson, P. & Bjarnason, I. Th. Reinterpretation of the RRRISP-77 Iceland shear-wave profiles. *Geophys. J. Int.* **126**, 166–172 (1996).
- Staples, R. K. *et al.* Faeroe-Iceland ridge experiment. 1. Crustal structure of northeastern Iceland. *J. Geophys. Res.* **102**, 7849–7866 (1997).
- Vogt, P. R. in *Structure and development of the Greenland-Scotland Ridge, New Methods and Concepts* (eds Bott, M. H. P., Saxov, S., Talwani, M. & Thiede, J.) 191–213 (Plenum, New York, 1983).
- Scott, D. R., Stevenson, D. J. & Whitehead, J. A. Jr Observations of solitary waves in a viscously deformable pipe. *Nature* **319**, 759–761 (1986).
- Olson, P. & Christensen, U. Solitary wave propagation in a fluid conduit within a viscous matrix. *J. Geophys. Res.* **91**, 6367–6374 (1986).
- McDougall, I., Kristjánsson, L. & Saemundsson, K. Magnetostratigraphy and geochronology of northwest Iceland. *J. Geophys. Res.* **89**, 7029–7060 (1984).
- Watkins, N. D. & Walker, G. P. L. Magnetostratigraphy of eastern Iceland. *Am. J. Sci.* **277**, 513–584 (1977).
- Albers, M. Channeling of plume flow beneath mid-ocean ridges. *Earth Planet. Sci. Lett.* **187**, 207–220 (2001).
- Cannat, M. *et al.* Mid-Atlantic Ridge–Azores hotspot interactions: along-axis migration of a hotspot-derived event of enhanced magmatism 10 to 4 Ma ago. *Earth Planet. Sci. Lett.* **173**, 257–269 (1999).
- Vogt, P. R. Global magmatic episodes: new evidence and implications for the steady-state mid-oceanic ridge. *Geology* **7**, 93–98 (1979).
- Sandwell, D. & Smith, W. H. F. Marine gravity from Geosat and ERS-1 altimetry. *J. Geophys. Res.* **102**, 10039–10054 (1997).
- DeMets, C., Gordon, R. G., Argus, D. F. & Stein, S. Effect of recent revisions to the geomagnetic reversal time scale on estimates of current plate motions. *Geophys. Res. Lett.* **21**, 2191–2194 (1994).
- McKenzie, D. & Bickle, M. J. The volume and composition of melt generated by extension of the lithosphere. *J. Petrol.* **29**, 625–679 (1988).
- Parker, R. L. The rapid calculation of potential anomalies. *Geophys. J. R. Astron. Soc.* **31**, 447–455 (1973).
- Wessel, P. & Smith, W. H. F. New version of the Generic Mapping Tools released. *Eos* **76**, 329 (1995).

Acknowledgements

Discussions with D. Lizarralde motivated much of the early work of this study. I also appreciate valuable comments by C. Leshner, J.-G. Schilling and D. Sparks. Figures 1, 3 and 4 were produced using Generic Mapping Tools³¹. Funding was provided by NSF-OCE.

Correspondence and requests for materials should be addressed to the author (e-mail: gito@geology.ucdavis.edu).

Earliest evidence for efficient oral processing in a terrestrial herbivore

Natalia Rybczynski* & Robert R. Reisz†

* Duke University, Department of Biological Anthropology and Anatomy, Box 90383, Durham, North Carolina 27708-0383, USA

† University of Toronto in Mississauga, Department of Zoology, 3359 Mississauga Road, Mississauga, Ontario L5L 1C6, Canada

Herbivores can increase their digestion rate by mechanically reducing particle size through oral trituration¹. Groups of terrestrial vertebrates with the greatest capacity to reduce tough plant foods orally are also the most abundant and diverse, as exemplified by ornithomorph dinosaurs during the Mesozoic and extant artiodactyl and perissodactyl mammals². Thus, the effective oral processing of high-fibre plant material seems to represent an evolutionary innovation of both functional and macroevolutionary significance. However, evidence for oral processing is poorly documented in the fossil record, especially during the initial stages of terrestrial vertebrate diversification^{3,4}. Here we report on the basal anomodont *Suminia getmanovi*, the only known Palaeozoic vertebrate in which unequivocal specializations in its cranium and teeth for high-fibre herbivory are well preserved. We propose that the capacity to comminute tough plant foods was critical to the diversification of anomodonts, the most diverse, widely dispersed and abundant group of Palaeozoic terrestrial vertebrates, and to the onset of modern terrestrial ecosystems.

One of the most significant evolutionary events in the history of life on land is the development of the modern pyramidal trophic structure in which terrestrial plants support a large number of herbivores, which in turn supports a relatively small number of predators⁴. Among vertebrates, this trophic organization was not fully developed until the Upper Permian (260 Myr ago) of the

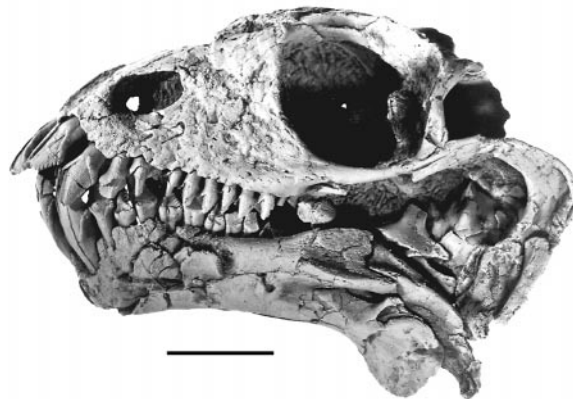


Figure 1 Skull of *Suminia getmanovi*, PIN 2212/62. Scale, 1 cm.